Self-Diffusion and Transport Diffusion of Light Gases in Metal-Organic Framework Materials Assessed Using Molecular Dynamics Simulations

Anastasios I. Skoulidas[†,§] and David S. Sholl*[,†,‡]

National Energy Technology Laboratory, Pittsburgh, Pennsylvania 15236, and Department of Chemical Engineering, Carnegie Mellon University, Pittsburgh, Pennsylvania 15213

Received: April 6, 2005; In Final Form: June 15, 2005

Metal-organic framework (MOF) materials pose an interesting alternative to more traditional nanoporous materials for a variety of separation processes. Separation processes involving nanoporous materials can be controlled by either adsorption equilibrium, diffusive transport rates, or a combination of these factors. Adsorption equilibrium has been studied for a variety of gases in MOFs, but almost nothing is currently known about molecular diffusion rates in MOFs. We have used equilibrium molecular dynamics (MD) to probe the self-diffusion and transport diffusion of a number of small gas species in several MOFs as a function of pore loading at room temperature. Specifically, we have studied Ar, CH_4, CO_2, N_2, and H_2 diffusion in MOF-5. The diffusion of Ar in MOF-2, MOF-3, and Cu−BTC has been assessed in a similar manner. Our results greatly expand the range of MOFs for which data describing molecular diffusion is available. We discuss the prospects for exploiting molecular transport properties in MOFs in practical separation processes and the future role of MD simulations in screening families of MOFs for these processes.

1. Introduction

Nanoporous materials such as zeolites and activated carbons have for years formed the basis of many industrial adsorption and separation processes.[1,2] Many of these processes are equilibrium-based and exploit the high adsorption selectivities that nanoporous materials can exhibit. An equally important class of processes are those that are kinetically based. These processes exploit differences in transport properties between molecular species adsorbed inside nanopores. The purification of N_2 from air using carbon molecular sieves is one example of a kinetically based process.[2] The distinction between these two classes of processes is of course not absolute. The effectiveness of membrane-based processes, for example, relies on both solubility differences, an equilibrium property, and diffusivity differences, a transport property.[3] The point of this discussion is to highlight the need to understand both adsorption and diffusion characteristics of any new (or old) nanoporous material to fully explore potential applications of that material in separation processes.

Metal-organic framework (MOF) materials have emerged as a fascinating addition to the known families of nanoporous materials. MOFs are crystalline materials that combine metal-organic complexes with organic "linker" species to create highly porous frameworks. Several recent review articles are available that describe structural and synthetic issues related to MOFs.[4−6] One attractive property of MOFs relative to zeolites or activated carbons is that their synthesis can be tailored with relatively direct control to generate multiple materials with systematically varying pore sizes and functionalities.

A variety of studies have examined the properties of MOFs and related materials for gas adsorption,[6] including the potential of these materials for hydrogen storage[7,8] and methane storage.[9] These studies provide insight into possible equilibrium-based applications of MOFs for gas separations, although information on multicomponent adsorption equilibrium is still lacking. It is useful to note that ideal adsorbed solution theory (IAST)[2,10] has been found to give accurate predictions of multicomponent adsorption in many zeolites,[11] and it seems likely that this observation will also apply to adsorption in the open pore spaces of many MOFs.

In contrast to the growing body of data related to adsorption equilibrium in MOFs, extremely little information is available regarding molecular transport in the same materials. As described above, knowledge of transport kinetics is vital to assess the potential of any nanoporous material over a full range of separation processes. The only information currently available on molecular diffusion in MOFs comes from computational simulations; we know of no experimental data. Two studies that appeared essentially simultaneously have applied molecular modeling to simulate diffusion in MOFs.[12,13] Sarkisov, Düren, and Snurr used molecular dynamics (MD) to examine the self-diffusion of methane, *n*-pentane, *n*-hexane, *n*-heptane, and cyclohexane in MOF-5 (also known as IRMOF-1), each at low loadings.[12] This type of calculation describes the transport rate of individual, isolated adsorbates. One of us used MD to examine the diffusion of Ar in another MOF, Cu−BTC.[13] This study probed the dependence of self-diffusion and transport diffusion of Ar over a wide range of pore loadings at room temperature. The transport diffusivity (defined more fully below) is the transport quantity relevant to the macroscopic nonequilibrium transport exploited in kinetic-based separation processes involving nanoporous materials. A fundamental property of nanoporous materials is that the self- and transport diffusivities for adsorbed species are equal only in the regime of dilute pore loadings.[14,15] At moderate and high pore loadings, these two

* Author to whom correspondence should be addressed. E-mail: sholl@andrew.cmu.edu.
† National Energy Technology Laboratory.
‡ Carnegie Mellon University.
§ Current address: ExxonMobil Research and Engineering, 3225 Gallows Rd., Fairfax, VA 22037.

10.1021/jp051771y CCC: $30.25
Published on Web 08/02/2005

diffusivities can differ markedly.[16,17] For Ar in Cu−BTC, for example, the two diffusivities differ by almost 2 orders of magnitude at high pore loadings.[13] One of the main conclusions from these initial studies is that the diffusion characteristics of small molecules inside MOFs are quite similar to the analogous quantities in zeolites in both magnitude and mechanism.[12,13]

There is growing evidence to suggest that current molecular models can accurately describe the properties of adsorbed gases in MOFs. Vishnyakov et al. compared simulated Ar adsorption isotherms at 77 K with high-resolution experimental data.[18] The universal force field (UFF), a general purpose force field describing interatomic interactions,[19] was found to predict the isotherm with reasonable accuracy. Düren and co-workers compared similar calculations using the UFF and Dreiding force fields with experimental adsorption isotherms for CH_4 in MOF-5 and IRMOF-6 at room temperature and found very good agreement between the resulting isotherms.[9] Recent studies have also used molecular models to examine H_2 adsorption in MOFs.[20,21] Since no experimental data is available for diffusion in MOFs, we cannot directly comment on the accuracy of the modeling studies cited above. It is useful in this context, however, to point out that such comparisons have been made using similar computational simulations for molecular diffusion in zeolites and excellent agreement has been found with experiments for both self-diffusion[15,22] and transport diffusion.[23,24] These studies provide at least some support for the view that demonstrating the accuracy of a force field for adsorption in a nanoporous material should also imply a reasonable level of confidence in the same force field for predicting diffusive properties. There are some examples of bulk fluids, notably polar fluids, for which simulations that successfully reproduce structural properties do not necessarily reproduce dynamic properties.[25,26] However, in general, whenever experimental equilibrium properties such as adsorption isotherms have been reproduced by simulations, it has been observed that dynamic simulations based on the same interatomic potentials are also reliable. We believe this will be the case in the present study. These considerations point to computational simulations as being a useful tool for expanding our limited knowledge of molecular diffusion in MOFs.

In this paper, we extend the two previous studies of molecular diffusion in two important directions. First, we characterize the loading-dependent diffusion of a number of gas species in a single material, MOF-5. The work of Sarkisov et al.[12] examined a series of *n*-alkanes in this material but only at dilute loadings. Our results are the first calculations to explore how differences in molecular size and adsorption affinity affect molecular diffusion as a function of pore loading in an MOF. Second, we compare the diffusion of a single species, Ar, in several MOFs, specifically, in MOF-2, MOF-3, MOF-5, and Cu−BTC. In each material, the role of pore loading is explored. Because the pore structure of MOFs can be tailored with relative ease, it would be extremely helpful to develop general insights into the connections between these pore structures and the resulting diffusion of adsorbed molecules. Our results represent a first step toward this goal.

We have used MD calculations to probe both the self-diffusion and transport diffusion of adsorbed molecules in MOFs. These two diffusivities have been defined and extensively discussed elsewhere,[13−16,27−29] but we review the most salient facts here for completeness. We only consider here examples in which just one species of adsorbate is present, although appropriate generalizations of these quantities exist for multicomponent diffusion.[15,30]

The self-diffusivity, D_s, describes the motion of individual, tagged particles. In an isotropic three-dimensional material, the self-diffusivity is related to the mean-squared displacement of tagged particles after time t by the Einstein relation

$$D_s(c) = \lim_{t\to\infty} \frac{1}{6t}\langle|\vec{\mathbf{r}}(t) - \vec{\mathbf{r}}(0)|^2\rangle \tag{1}$$

Here, $\vec{\mathbf{r}}(t)$, is the position of a tagged particle at time t, and the angular brackets indicate an ensemble average. The self-diffusivity is also sometimes referred to as the tracer diffusivity.[31]

The transport diffusivity, D_t, is defined as the proportionality constant relating a macroscopic flux to a spatial concentration gradient in Fick's law

$$J = -D_t(c)\nabla c \tag{2}$$

The transport diffusivity is also commonly referred to as either the Fickian diffusivity,[32,33] the chemical diffusivity,[31] or the collective diffusivity.[34] It is often convenient to define the transport diffusivity in terms of the corrected diffusivity, D_0, via

$$D_t(c) = D_0(c)\left(\frac{\partial \ln f}{\partial \ln c}\right)_T \tag{3}$$

In this expression, the partial derivative involving the adsorbate concentration, c, and the bulk phase fugacity, f, is known as the thermodynamic correction factor. This derivative is fully defined once the single-component adsorption isotherm is known. The corrected diffusivity also has alternative names; it is known as the jump diffusivity.[31] The corrected diffusivity is important in its own right because in the Maxwell−Stefan formulation of mass transfer by diffusion the corrected diffusivity is equal to the Maxwell−Stefan diffusivity in single-component systems.[35]

The self-, transport, and corrected diffusivities are all, in general, functions of concentration, and they are only equal in the limit of dilute concentrations. In extreme cases, the self- and transport diffusivities can vary by orders of magnitude.[16,17] This observation underscores the value of characterizing these two diffusivities independently. In applications where it is necessary to accurately describe net mass transfer under nonequilibrium conditions, such as in modeling of membranes or cyclic separation methods such as pressure swing adsorption, it is the transport diffusivity that is of greatest interest.

Section 2 describes the interatomic potentials that we used in our simulations of adsorption and diffusion in MOFs and the details of our simulation methods. The adsorption and diffusion of Ar, CH_4, CO_2, N_2, and H_2 in MOF-5 at room temperature are described in section 3. The effect of varying the adsorbent material is explored in section 4 by assessing Ar diffusion at room temperature in MOF-2, MOF-3, MOF-5, and Cu−BTC. In all cases, we describe the loading dependence of the self-, corrected, and transport diffusivities. The implications of our results for experimental measurements of diffusion in MOFs and for exploiting the transport properties of adsorbed species in MOFs in practical applications are discussed in section 5.

2. Simulation Methods and Interatomic Potentials

The metal-organic frameworks considered in this paper were modeled as rigid frameworks, with their atoms held fixed in their experimentally determined crystallographic positions.[12,13,18]

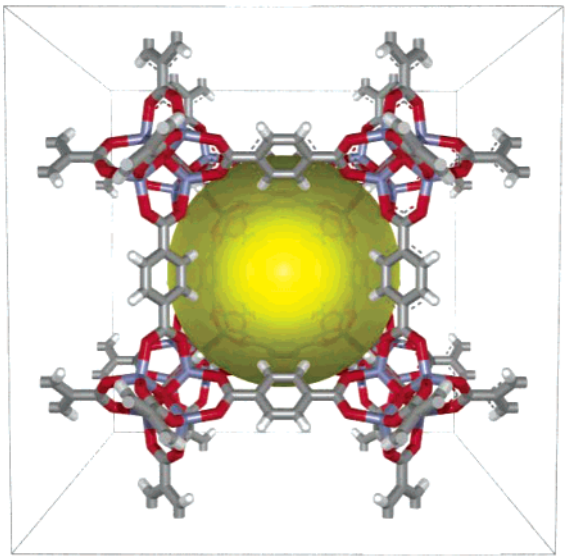

Figure 1. Schematic view of one unit cell of MOF-5. The large sphere represents the empty pore volume in the interior of the unit cell.

Cu−BTC has a cubic lattice with a unit cell dimension of 26.343 Å. The structure of Cu−BTC was taken from Chui et al.[36] The crystal structure of Chui et al. includes axial oxygen atoms bonded to the Cu atoms, which correspond to water ligands. We simulated dry Cu−BTC with these oxygen atoms removed.[13,18] Cu−BTC has a three-dimensional channel structure connecting a system of tetrahedral-shaped cages accessible through small windows. The central cavity of the unit cell in Cu−BTC is inaccessible to molecules at moderate temperatures and pressures.[13] MOF-5 has also a cubic framework with a unit cell dimension of 25.669 Å.[37] Figure 1 shows one unit cell of MOF-5. The empirical formula of MOF-5 is $C_{6.40}H_{3.20}O_{3.47}Zn_{1.07}$. MOF-5 too has a three-dimensional channel network connecting the large cages at the center of each unit cell. Similar to Cu−BTC, the central cavity of MOF-5 is not accessible for adsorption at moderate temperatures and pressures. MOF-5 is also referred to as IRMOF-1 (IRMOF from the expression isoreticular metal-organic framework[5]). We used the crystallographic data reported by Li et al.[38] MOF-2 has a monoclinic crystal structure with channels running across the (100) and (001) crystallographic directions.[39] It crystallizes in the $P2_1/n$ space group with dimensions $a = 6.718$ Å, $b = 15.488$ Å, $c = 12.43$ Å, and $\beta = 102.83°$. The empirical formula of MOF-2 is Zn(BDC)·(DMF)(H_2O) (BDC = 1,4-benzenedicarboxylate, DMF= *N*,*N*′-dimethylformamide). Li et al. have shown that the crystal structure of MOF-2 remains unchanged upon removal of the DMF molecules.[39] Simulations of adsorption and diffusion in MOF-2 were performed with the guest molecules removed. Finally, MOF-3 has a triclinic crystal structure with a three-dimensional (3D) pore network.[37] The dimensions of the crystal cell are $a = 9.726$ Å, $b = 9.911$ Å, $c = 10.45$ Å, $\alpha = 99.72°$, $\beta = 102.83°$, and $\gamma = 108.42°$. The empirical formula of MOF-3 is $Zn_3(BDC)_3$·$6CH_3OH$. Similar to MOF-2, we simulated MOF-3 with the guest molecules (methanol) present after synthesis removed.

To model Ar, CH_4, and H_2, we used a spherical Lennard-Jones potential with parameters described previously.[29] For CO_2, we used the EPM2 model, which is an all-atom Lennard-Jones potential with atomic charges to approximate CO_2's quadrupole moment.[40] A similar potential was used for N_2.[41] Interactions between adsorbed molecules and the MOFs were modeled using pairwise interactions between adsorbates and each atom in the MOF. For Ar, CH_4, and H_2, only Lennard-Jones interactions were considered for these interactions. The parameters for these interactions were taken from the UFF potential[19] except for CH_4 in MOF-5 where we used the Dreiding potential[42] following Duren et al.[9] Mixed-atom interactions were defined using the Lorenz−Berthelot mixing rules. Charges were added for each atom in the MOF-5 unit cell for the simulations involving CO_2 and N_2. The atomic charges of MOF-5 were estimated with DMol[3] based on density functional theory B3LYP calculations.

In both grand canonical Monte Carlo (GCMC) and equilibrium molecular dynamics (EMD) simulations, a cutoff distance of 17 Å was used for the Lennard-Jones interactions. Long-range corrections were included in the adsorbate−MOF interactions by assuming the MOF was isotropic at distances beyond the cutoff. This application of long-range corrections inside what is an intrinsically structured material is of course an approximation, a point discussed carefully by Macedonia and Maginn.[43] The potentials used in the EMD simulations were cut and shifted at the cutoff distance. The interactions with the MOFs were pretabulated on a 0.2-Å grid. During the simulations, a 3D cubic Hermite polynomial interpolation scheme was used to calculate the potential at each point in space.[29] A direct evaluation of the electrostatic interaction between the adsorbates was employed with a cutoff distance of 25 Å for CO_2 and N_2. This approach is possible because the quadrupole interactions between these molecules converge rapidly as the cutoff distance is increased. The electrostatic potential and forces due to interactions between the quadrupolar species and MOF-5 were pretabulated using a direct evaluation of the atomic charge−charge interactions employing 515 MOF-5 unit cells.[44]

Adsorption isotherms of each molecule were computed using GCMC simulations.[45,46] The chemical potential of each bulk gas was related to its pressure by an equation of state. For CH_4, Ar, and H_2, we used the virial equation of state, while for CO_2 and N_2 we have used the BWR equation of state.[47] For CH_4, the virial expansion was taken up to the fourth virial coefficient using the coefficients determined experimentally by Doulsin et al.[48] For Ar and H_2, virial coefficients were fitted to experimental data by NIST.[49] A minimum $2 \times 2 \times 2$ unit cell simulation box was used for MOF-5 and Cu−BTC, $6 \times 3 \times 3$ for MOF-2, and $5 \times 4 \times 4$ for MOF-3. At the lowest densities, the size of the simulation volume was increased as to contain at least 50 particles during the simulations. At least 2 million equilibration and 5 million production steps were used for each loading. At the highest loadings, as many as 10 million equilibration and 25 million production steps were used.

The self- and corrected diffusivities of adsorbed molecules were computed using EMD simulations. The details of applying this technique to similar crystalline nanoporous materials have been reported previously.[28,29] Corrected diffusivities in nanoporous materials can be calculated from EMD simulations using an efficient method first described by Theodorou et al.[50,51] This method uses an Einstein relationship similar to eq 1 that measures the mean-squared displacement of the center of mass of the adsorbed molecules

$$D_0 = \frac{1}{6N} \lim_{t \to \infty} \frac{1}{t} \langle || \sum_{l=1}^{N} (\vec{\mathbf{r}}_l(t) - \vec{\mathbf{r}}_l(0)) ||^2 \rangle \qquad (4)$$

Here, N is the number of adsorbates in the simulation volume, and the average is taken over a large number of independent trajectories. Equation 4 easily can be generalized to determine the x, y, or z component of a diffusivity by replacing the factor of 6 by a factor of 2 and by using the desired component of position instead of the position vectors.[50,52] The orientationally

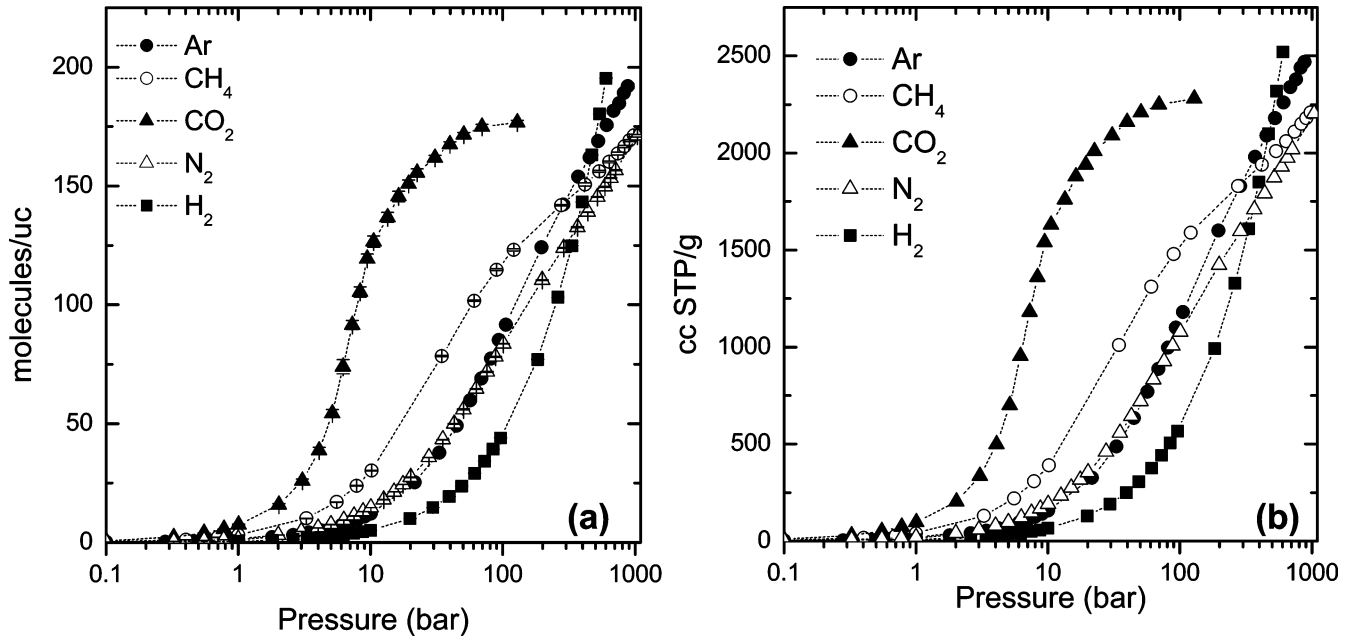

Figure 2. Adsorption isotherms of Ar, CH_4, CO_2, N_2, and H_2 in MOF-5 computed using GCMC in (a) molecules/unit cell and (b) cm^3 (STP)/g adsorbent.

averaged diffusivity shown in eq 4 is related to the individual components of the diffusivities by $D_0 = (D_{0,x} + D_{0,y} + D_{0,z})/3$. For each molecule studied, we have performed 20 independent MD simulations for each loading, with a simulation length varying from 0.8 to 2.5 ns after shorter EMD simulations were used to equilibrate each system. The transport diffusivity was calculated from eqs 3 and 4 after determining the thermodynamic correction factor in eq 3 from the adsorption isotherms predicted by GCMC.

3. Ar, CH_4, CO_2, N_2, and H_2 Adsorption and Diffusion in MOF-5

In this section, we describe the room-temperature adsorption and diffusion of five gases, Ar, CH_4, CO_2, N_2, and H_2, in a single metal-organic framework material, MOF-5. The absolute adsorption isotherms computed using GCMC are shown in Figure 2 in both molecules/unit cell (Figure 2a) and in cm^3 (STP)/g adsorbent (Figure 2b). As is observed in silica zeolites,[28,41,44] CO_2 adsorbs considerably more strongly than the other gases, and H_2 adsorbs considerably more weakly.

Our simulations of CH_4 used the same interaction potentials as in the earlier work of Duren et al.[9] We obtain results in very good agreement with experimental data when we use the same cutoff radius and simulation lengths as Duren et al. For example, we calculated an excess adsorption capacity of 220.2 cm^3 (STP) CH_4/g MOF-5 at 35 atm, which is in close agreement with experiment.[9] Unfortunately, this level of agreement decreases when we increase the cutoff radius from the value of 12.8 Å of Duren et al. to the value of our other simulations, 17 Å, and when long-range corrections are included. Performing the calculation in this way yields an excess adsorption capacity of 235.7 cm^3 (STP) CH_4/g MOF-5 at 35 atm. Thus, it appears that the Dreiding potential as used by Duren et al. slightly overestimates the adsorption strength of CH_4 in MOF-5. Our predictions for H_2 adsorption in MOF-5 (1.15 wt % H_2 at 20 bar) are in close agreement with experimental measurements at room temperature, where adsorption of ~1 wt % H_2 has been reported at 20 bar.[7]

Because of the large pore volume of MOF-5, the saturation capacity for each gas is large when compared to those of zeolites. It can be seen from Figure 2 that the saturation capacity for each species exceeds 200 molecules/unit cell. The large accessible pore volume is not necessarily useful for practical applications, since the more weakly adsorbing species only exhibit substantial pore filling at very high pressures. We return to the issues of practical gravimetric and volumetric measures of adsorption capacity below when we compare Ar adsorption in several MOFs.

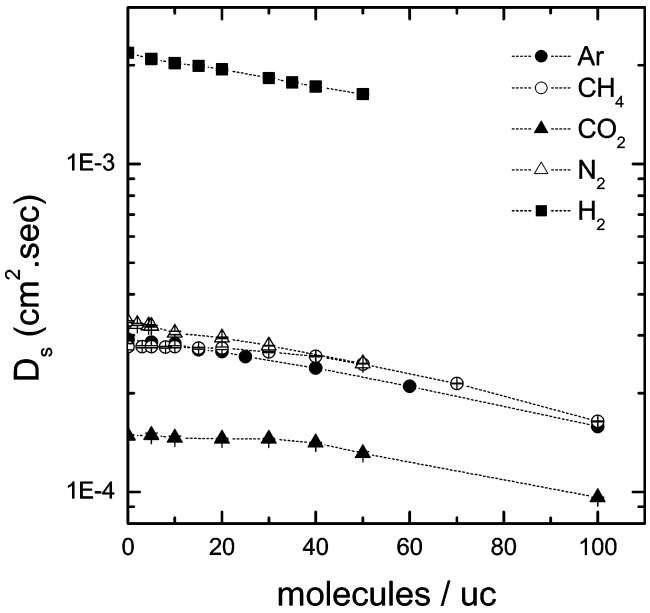

Figure 3. Self-diffusivities of Ar, CH_4, CO_2, N_2, and H_2 in MOF-5 at room temperature.

The room-temperature self-diffusivities of Ar, CH_4, CO_2, N_2, and H_2 in MOF-5 are shown in Figure 3. The concentration ranges probed in Figure 3 are modest compared to the saturation capacity of MOF-5, but for each species except CO_2 they correspond to large pressure ranges. At zero loading, the magnitude of the self-diffusivities is $H_2 > N_2 \approx CH_4 \approx Ar > CO_2$. The magnitude of each self-diffusivity is similar to those that have been reported in similar calculations for diffusion in silica zeolites.[27−29,41,44]

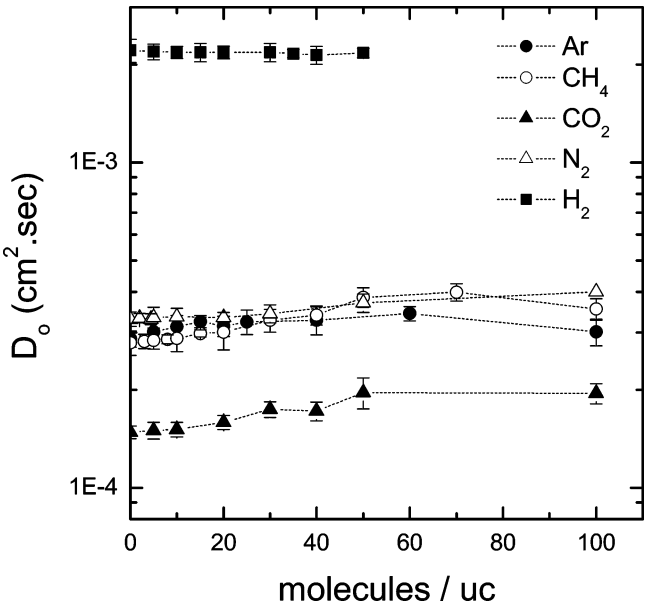

Figure 4. Corrected diffusivities of Ar, CH_4, CO_2, N_2, and H_2 in MOF-5 at room temperature.

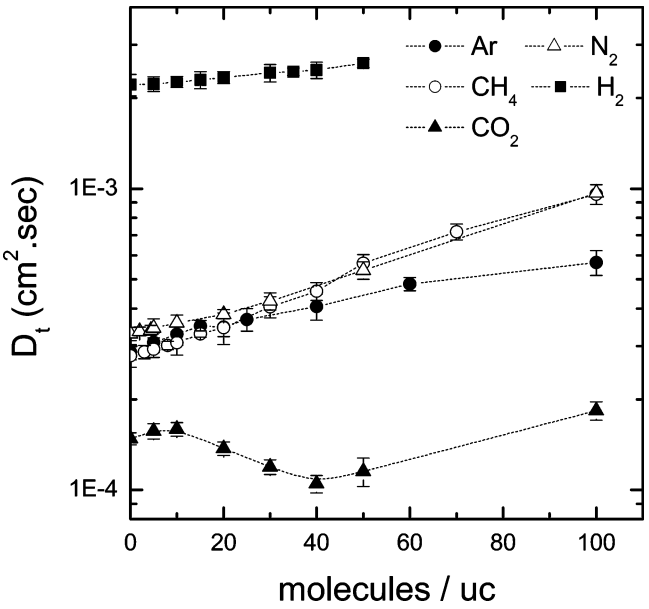

Figure 5. Transport diffusivities of Ar, CH_4, CO_2, N_2, and H_2 in MOF-5 at room temperature.

The concentration dependence of the self-diffusivity for each species in Figure 3 is similar, showing a moderate decrease with increasing concentration. This behavior is one of the most common forms of concentration dependence observed in nanoporous materials. This concentration dependence arises as a natural consequence of steric hindrance between diffusing molecules. Because our simulations only probed low and moderate pore loadings relative to the saturation capacity, the effect of concentration on D_s is weak.

Figure 4 shows the computed room-temperature corrected diffusivity, D_0, for Ar, CH_4, CO_2, N_2, and H_2 in MOF-5. In silica zeolites and carbon nanotubes where this quantity has been characterized previously,[16,23,27−29] D_0 is typically found to decrease as the pore loading is increased. In contrast, the corrected diffusivities in Figure 4 are either essentially constant or increase slightly as the pore loading increases. An interesting implication of these results is that over the large pressure range represented by our results treating D_0 as a constant would be a very good approximation. This approximation has been used widely in analysis of macroscopic diffusion data in nanoporous materials, but detailed studies have revealed only a small number of examples where this idea can be used with quantitative accuracy.[14,27,30]

By combining thermodynamic correction factors determined from our adsorption isotherms and the corrected diffusivities just discussed, we can determine the transport diffusivities of each gas in MOF-5. The resulting diffusivities are shown in Figure 5. For Ar, CH_4, N_2, and H_2, the concentration dependence is simple; the transport diffusivity increases monotonically as the pore loading is increased. This is a consequence of the corrected diffusivities being approximately independent of loading and the thermodynamic correction factors increasing monotonically with pressure. CO_2 is an unusual case in that the computed transport diffusivity is a nonmonotonic function of pore loading. This nonmonotonicity arises because the thermodynamic correction factor is nonmonotonic; the corrected diffusivity increases monotonically with loading (cf. Figure 4). For low pore loadings, the isotherm of CO_2 in MOF-5 rises in a slightly sublinear manner with respect to pressure, presumably due to weak repulsions between the adsorbed molecules. This causes the thermodynamic correction factor to be slightly less than 1 over this range of loadings. The nonmonotonic behavior of D_t for CO_2 is perhaps best described as a curiosity rather than a dramatic physical phenomenon; over the entire range of pore loadings that we examined, this diffusivity varies by less than a factor of 2.

4. Ar Adsorption and Diffusion in MOF-5, MOF-2, MOF-3, Cu−BTC, and Silicalite

In this section, we use Ar as a probe species to compare the room-temperature diffusion of a small gas species in several MOF materials. We have previously examined Ar diffusion in one MOF, Cu−BTC,[13] and in silicalite, a prototypical silica zeolite.[28] Here, we augment these results with calculations for Ar diffusion in MOF-2, MOF-3, and MOF-5. The computed room-temperature adsorption isotherms for Ar in each of these five materials are shown in Figure 6 in both cm^3 (STP)/g and cm^3 (STP)/cm^3. At low and moderate pressures, that is, up to a few tens of bars, all five materials exhibit quite similar adsorption capacities. At high pressures, the large-pore MOFs have large adsorption capacities compared to that of silicalite. If adsorption capacity is measured in cm^3 (STP)/g, then MOF-5 and Cu−BTC have similar high-pressure capacities for Ar, and this capacity is considerably larger than those in MOF-3 and MOF-2. If the adsorption is characterized in cm^3 (STP)/cm^3, then the ordering of the five materials is the same, but the quantitative distinction between the capacities of the two largest pore materials and MOF-3 and MOF-2 is less dramatic than when viewed in cm^3 (STP)/g.

The self-diffusivities of Ar in the five materials are shown in Figure 7. For each material except MOF-5, the pore loadings for which data are given in Figure 7 span the range from dilute loadings to loadings approaching the saturation capacity. For MOF-5, the data in Figure 7 represent gas pressures up to ∼100 atm. At zero loading, the diffusivities of Ar in these materials span less than an order of magnitude. The relative magnitude of the zero loading diffusivity cannot be linked in a simple way to pore size; the two smallest pore materials, MOF-2 and MOF-3, have the largest and smallest diffusivities of all five materials, respectively. Nonmonotonic variations in diffusivities at dilute loadings as the ratio of pore size to adsorbate size is varied are well-known in zeolites.[53,54]

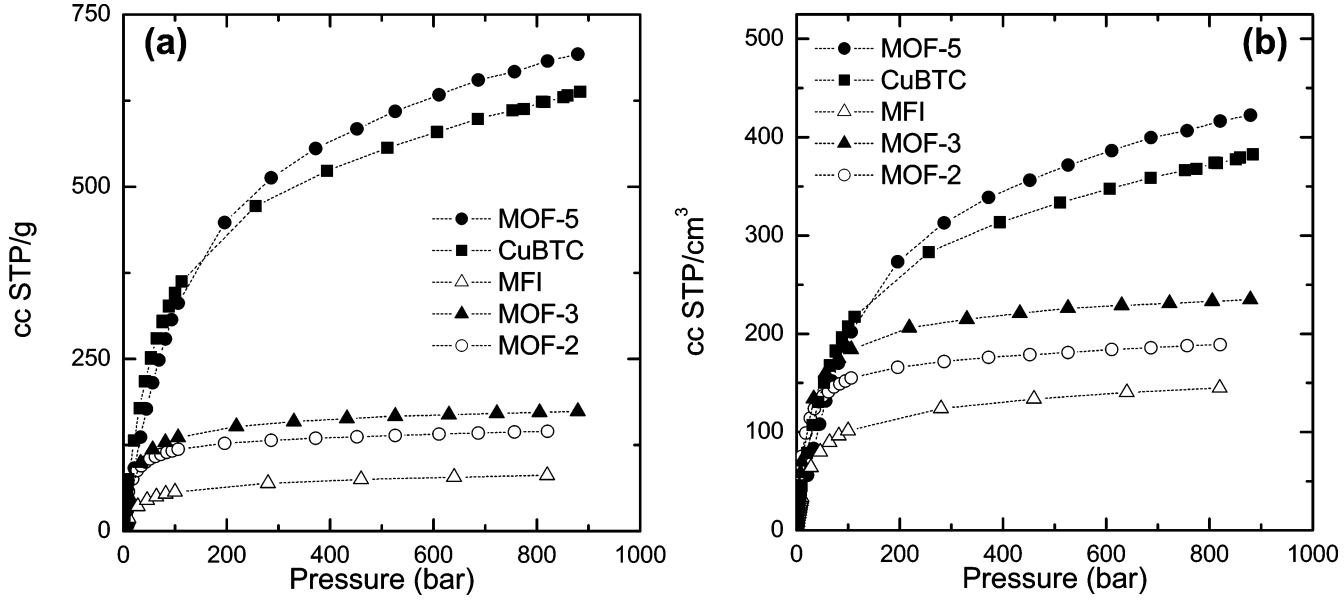

Figure 6. Ar isotherms for MOF-2, MOF-3, MOF-5, Cu−BTC, and silicalite (MFI) computed using GCMC in (a) cm^3 (STP)/g adsorbent and (b) cm^3 (STP)/cm^3 adsorbent.

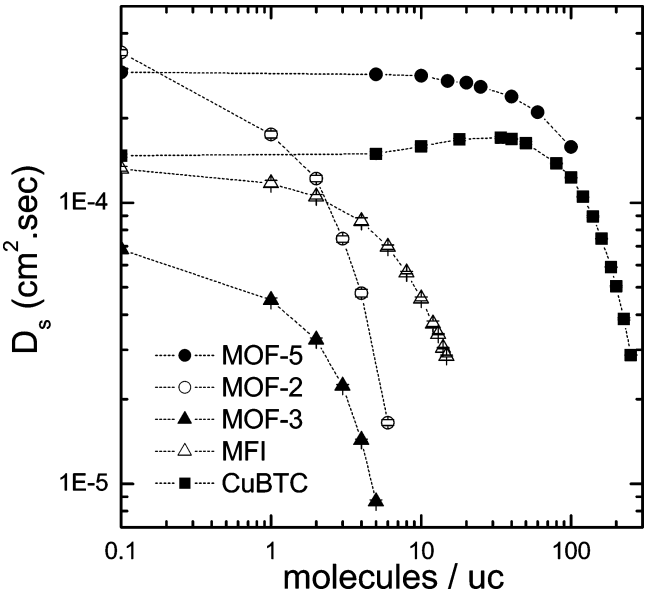

Figure 7. Self-diffusivities of Ar in MOF-5, MOF-2, MOF-3, Cu−BTC, and silicalite (MFI) at room temperature.

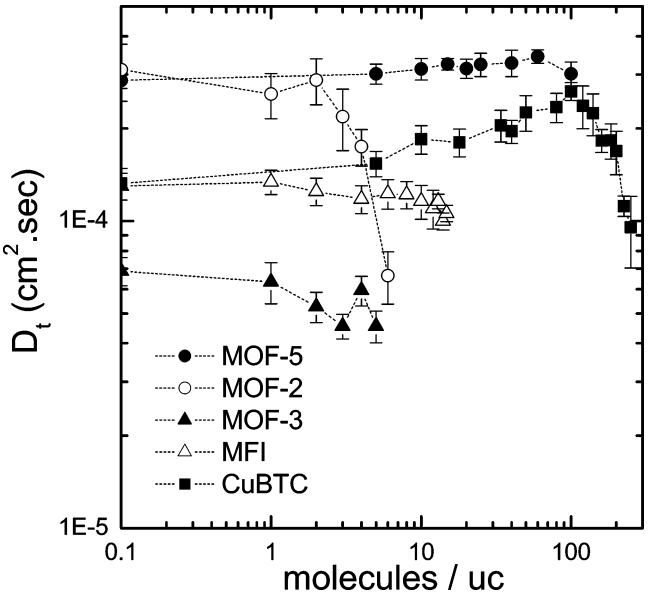

Figure 8. Corrected diffusivities of Ar and CH_4 in MOF-5, MOF-2, MOF-3, Cu−BTC, and silicalite (MFI) at room temperature.

The concentration dependencies of D_s for Ar in MOF-2, MOF-3, MOF-5, and silicalite are similar, showing a monotonic decrease with increasing pore loading. This decrease in the diffusivity becomes quite marked as the pore loading approaches the saturation capacity, reflecting the severe steric hindrance posed to a diffusing molecule by other adsorbed molecules in this limit. The diffusion of Cu−BTC is an interesting exception to the trend seen in the other four materials. In Cu−BTC, the self-diffusivity initially increases with loading, then decreases strongly for loadings approaching the saturation capacity. This behavior has been discussed previously.[13] Briefly, it occurs because the rate-limiting step for diffusion of Ar in Cu−BTC is the hopping of Ar atoms between cages within the material that are separated by a considerable energetic barrier. The presence of nearby Ar atoms reduces this energetic barrier through a cooperative effect. A similar mechanism has been shown to underlie the nonmonotonic self-diffusivity of methane in the silica form of zeolite Linde type A.[55−57]

Figure 8 shows the computed corrected diffusivities of Ar in the five nanoporous materials. It is interesting to analyze these corrected diffusivities in terms of their relationships with Ar self-diffusion in each material. The differences between self- and corrected diffusivities arise due to interadsorbate correlations.[28,30] When the motions of different adsorbates are strongly correlated, the corrected diffusivity differs strongly from the self-diffusivity. One extreme example of this phenomenon is the diffusion of small molecules in carbon nanotubes; in this case the two diffusivities can differ by orders of magnitude.[16,17,58] The diffusion of Ar in silicalite and in MOF-3 shows strong correlation effects, with the corrected diffusivity decreasing very weakly as a function of increasing loading over the entire range of possible pore loadings. The correlation effects on Ar diffusion in MOF-2 and Cu−BTC are weaker in the sense that the loading dependence of the corrected diffusivity is quite similar to the self-diffusivity over the entire range of pore loadings. In MOF-5, the correlation effects are not dramatic, but we note again that our data only probe low and moderate

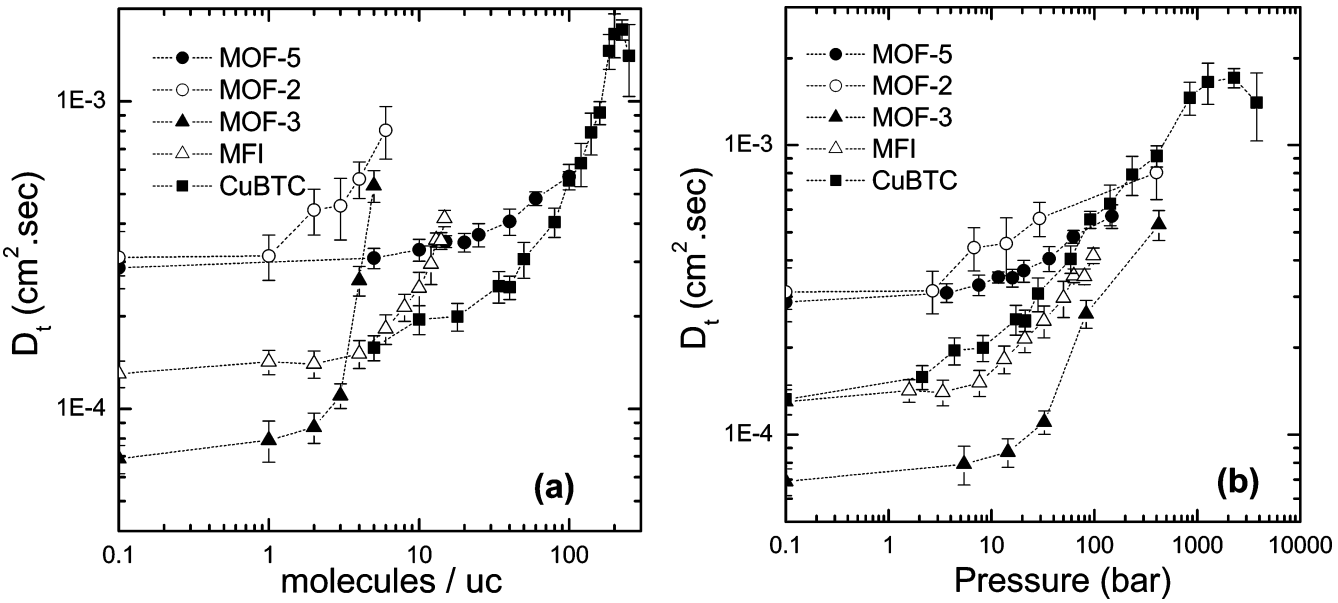

Figure 9. Transport diffusivities of Ar in MOF-5, MOF-2, MOF-3, Cu−BTC, and silicalite (MFI) at room temperature.

pore loadings in this material. As with previous simulations of self- and corrected diffusivities in silica zeolites, the data presented here provide a challenge to any phenomenological efforts to predict the dependence of correlation effects based on pore topology.[16,23,27−29]

The computed room-temperature transport diffusivities of Ar in MOF-2, MOF-3, MOF-5, Cu−BTC, and silicalite are shown in Figure 9. In this figure, the results are presented both in terms of the adsorbate density in molecules/unit cell (Figure 9a) and also in terms of the bulk gas pressure needed to generate these adsorbate densities (Figure 9b). The latter figure can also be used to interpret the data for self- and corrected diffusion in Figures 7 and 8 in terms of the gas-phase pressure. In each material, the transport diffusivity increases monotonically with loading at all experimentally meaningful pressures. Cu−BTC shows the widest variation in D_t with loading of any of the materials. In this case, the increasing trend for the corrected diffusivity couples with the growth in the thermodynamic correction factor with increasing loading to generate a strong dependence of D_t on loading. In the other four materials, the fact that the corrected diffusivity either is relatively constant or decreases with loading moderates the increase in D_t due to the thermodynamic correction factor.

5. Discussion

We have presented computational simulations of the diffusion of several light gases in several MOFs. In each case, we have separately determined the self-diffusivity, corrected diffusivity, and transport diffusivity as a function of pore loading at room temperature. Our results greatly expand the scope of data that was previously available describing molecular diffusion in MOFs.[12,13] Our results support the conclusions of previous work that the diffusion coefficients of molecules in MOFs are similar in magnitude to the analogous diffusion coefficients in zeolites. Below, we discuss future prospects for measuring molecular diffusion in MOFs experimentally, the development of practical separation processes involving MOFs, and mechanisms that characterize diffusion in MOFs.

In the Introduction, we emphasized that no experimental data is currently available measuring molecular diffusivities in MOFs. One implication of our results is that the methods that have been widely applied to measuring diffusivities in zeolites should be just as applicable to MOFs, since MOF crystals of appreciable size are readily synthesized and the predicted diffusivities are similar in magnitude to those in zeolites. Comparisons between our calculated diffusivities and experimental measurements could be made most directly if pulsed field gradient NMR or quasi-elastic neutron scattering (QENS) were used to measure self-diffusion.[15,22] QENS could also be used to directly measure transport diffusivities.[23,24] Other experimental techniques such as single-crystal permeation could also give extremely interesting insights and can be directly compared to calculations of the type that we have reported here.[27] Although the available evidence from simulations of adsorption equilibrium indicates that the simulation methods that we have used here can be quite accurate for describing molecular adsorption in MOFs, making direct comparisons of predicted diffusivities with experimental measurements would be of great value.

We now consider how knowledge of molecular diffusivities in MOFs might be used to screen MOFs for use in various practical processes. In applications involving gas storage, the primary quantity of interest is the adsorption capacity under various conditions. The main requirement on diffusion rates in this venue is that diffusion not be so slow as to limit charging or discharging times. This requirement also applies to equilibrium-based separation processes[2]. The fact that diffusivities in MOFs are similar to those in zeolites strongly suggests that MOFs will meet this requirement.

A more interesting set of applications to consider are those that are to some extent kinetically based, as discussed in the Introduction. In these cases, reliable means of estimating transport rates are crucial to screen a MOF (or, more usefully, a family of MOFs) as a potential adsorbent or membrane material. Practical design of adsorbent-based separation processes often uses a linear driving force model to simplify the complexities of diffusion in nanoporous materials into a tractable form.[2,59,60] The similarity between diffusion in MOFs and zeolites suggests that, at least for very crude estimates of process performance, using linear driving force coefficients typical for zeolites in combination with adsorption parameters measured for specific MOFs would be a reasonable preliminary approximation to modeling process performance using MOFs. There are, of course, more accurate mathematical descriptions that exist for specific processes. The information available from

the types of simulations that we have reported here is well-suited to assessing the possible performance of nanoporous materials as membranes[16,61] and could readily be connected with detailed models of other processes.[62] Smit and Krishna have recently discussed the potential for using molecular modeling methods in aiding process design involving zeolites.[11] These ideas could potentially find even more powerful use in considering possible uses of MOFs, where extensive experimental testing of the large number of possible MOF structures may be prohibitively time-consuming.

We conclude with some qualitative comments regarding the mechanism of molecular diffusion in MOFs. Diffusion in mesoporous and microporous materials is typically discussed in terms of contributions from Knudsen diffusion and surface (or configurational) diffusion.[2,3] In Knudsen diffusion, adsorbate−wall collisions dominate over adsorbate−adsorbate collisions, but adsorbate trajectories between wall collisions are viewed as being effectively unperturbed by nearby walls.[63,64] In surface diffusion, adsorbates are viewed as being in constant contact with the walls. The latter view is clearly appropriate for molecular diffusion in zeolites, where in many instances the pore diameters are similar in magnitude to the size of the adsorbed species. In some instances, Knudsen diffusion has been invoked to describe diffusion in pores that are larger than those in zeolites but comparable to those in the most porous MOFs.[65] We assert that Knudsen diffusion is not an appropriate description of molecular diffusion in MOFs. Although MOFs can have large open volumes inside their frameworks,[5] these open volumes are only filled with adsorbates at very high pressures. The effective pore size available to adsorbed molecules is defined by regions inside the MOF where the adsorbate's potential energy lies within thermal energies of the binding energy associated with the lowest-energy binding sites. The potential-energy maps of Vishnyakov et al.[18] are an excellent example of this general observation. The local pore diameters associated with these effective pore regions are of molecular dimensions. Thus, it is fair to say that diffusion of molecules in MOFs will be dominated by motions where the adsorbed species remain in close contact with the surfaces defined by the pore structure throughout their diffusion.

A challenge remaining in understanding molecular diffusion in MOFs and related materials is to provide detailed insight into the differences between self- and transport diffusion at a microscopic level. This task has been tackled by a number of authors for pure liquids.[66−68] Future exploration of the connections between this existing work on pure liquids and the more complex situation of molecules adsorbed inside a porous structure seems likely to yield useful insights.

Acknowledgment. D.S.S. was partially supported by the National Science Foundation (CTS-0413027) and is a National Energy Technology Laboratory Faculty Fellow. Many helpful conversations with Professor J. K. Johnson are gratefully acknowledged.

References and Notes

(1) Ruthven, D. M. *Principles of Adsorption and Adsorption Processes*; John Wiley: New York, 1984.
(2) Yang, R. T. *Gas Separation by Adsorption Processes*; Butterworth: Boston, MA, 1987.
(3) Wesselingh, J. A.; Krishna, R. *Mass Transfer in Multicomponent Mixtures*; Delft University Press: Delft, The Netherlands, 2000.
(4) Eddaoudi, M.; Kim, J.; Rosi, N.; Vodak, D.; Wachter, J.; O'Keefe, M.; Yaghi, O. M. *Science* **2002**, *295*, 469.
(5) Yaghi, O. M.; O'Keeffe, M.; Ockwig, N. W.; Chae, H. K.; Eddaoudi, M.; Kim, J. *Nature* **2003**, *423*, 705.
(6) Snurr, R. Q.; Hupp, J. T.; Nguyen, S. T. *AIChE J.* **2004**, *50*, 1090.
(7) Rosi, N. L.; Eckert, J.; Eddaoudi, M.; Vodak, D. T.; Kim, J.; O'Keeffe, M.; Yaghi, O. M. *Science* **2003**, *300*, 1127.
(8) Pan, L.; Sander, M. B.; Huang, X.; Li, J.; Smith, M.; Bittner, E.; Bockrath, B.; Johnson, J. K. *J. Am. Chem. Soc.* **2004**, *126*, 1308.
(9) Duren, T.; Sarkisov, L.; Yaghi, O. M.; Snurr, R. Q. *Langmuir* **2004**, *20*, 2683.
(10) Myers, A. I.; Prausnitz, J. M. *AIChE J.* **1965**, *11*, 121.
(11) Smit, B.; Krishna, R. *Chem. Eng. Sci.* **2003**, *58*, 557.
(12) Sarkisov, L.; Duren, T.; Snurr, R. Q. *Mol. Phys.* **2004**, *102*, 211.
(13) Skoulidas, A. I. *J. Am. Chem. Soc.* **2004**, *126*, 1356.
(14) Kärger, J.; Ruthven, D. *Diffusion in Zeolites and Other Microporous Materials*; John Wiley & Sons: New York, 1992.
(15) Keil, F. J.; Krishna, R.; Coppens, M. O. *Rev. Chem. Eng.* **2000**, *16*, 71.
(16) Skoulidas, A. I.; Ackerman, D. M.; Johnson, J. K.; Sholl, D. S. *Phys. Rev. Lett.* **2002**, *89*, 185901.
(17) Ackerman, D. M.; Skoulidas, A. I.; Sholl, D. S.; Johnson, J. K. *Mol. Simul.* **2003**, *29*, 677.
(18) Vishnyakov, A.; Ravikovitch, P. I.; Neimark, A. V.; Bulow, M.; Wang, Q. M. *Nano Lett.* **2003**, *3*, 713.
(19) Rappe, A. K.; Casewit, C. J.; Colwell, K. S.; Goddard, W. A., III; Skiff, W. M. *J. Am. Chem. Soc.* **1992**, *114*, 10024.
(20) Sagara, T.; Klassen, J.; Ganz, E. *J. Chem. Phys.* **2004**, *121*, 12543.
(21) Garberoglio, G.; Skoulidas, A. I.; Johnson, J. K. *J. Phys. Chem. B* **2005**, *109*, 13094.
(22) Snurr, R. Q.; Kärger, J. *J. Phys. Chem. B* **1997**, *101*, 6469.
(23) Jobic, H.; Skoulidas, A. I.; Sholl, D. S. *J. Phys. Chem. B* **2004**, *108*, 10613.
(24) Chong, S.-S.; Jobic, H.; Plazanet, M.; Sholl, D. *Chem. Phys. Lett.* **2005**, *408*, 157.
(25) Chialvo, A. A.; Kettler, M.; Nezbeda, I. *J. Phys. Chem. B* **2005**, *109*, 9736.
(26) Zwanzig, R. *J. Chem. Phys.* **1963**, *38*, 1603.
(27) Skoulidas, A. I.; Sholl, D. S. *J. Phys. Chem. B* **2001**, *105*, 3151.
(28) Skoulidas, A. I.; Sholl, D. S. *J. Phys. Chem. B* **2002**, *106*, 5058.
(29) Skoulidas, A. I.; Sholl, D. S. *J. Phys. Chem. A* **2003**, *107*, 10132.
(30) Skoulidas, A. I.; Sholl, D. S.; Krishna, R. *Langmuir* **2003**, *19*, 7977.
(31) Uebing, C.; Gomer, R. *J. Chem. Phys.* **1994**, *100*, 7759.
(32) Auerbach, S. M. *Int. Rev. Phys. Chem.* **2000**, *19*, 155.
(33) Sholl, D. S. *Ind. Eng. Chem. Res.* **2000**, *39*, 3737.
(34) Mak, C. H.; Andersen, H. C.; George, S. M. *J. Chem. Phys.* **1988**, *88*, 4052.
(35) Krishna, R.; van den Broeke, L. J. P. *Chem. Eng. J.* **1995**, *57*, 155.
(36) Chui, S. S. Y.; Lo, S. M. F.; Charmant, J. P. H.; Orpen, A. G.; Williams, I. D. *Science* **1999**, *283*, 1148.
(37) Eddaoudi, M.; Li, H. L.; Yaghi, O. M. *J. Am. Chem. Soc.* **2000**, *122*, 1391.
(38) Li, H.; Eddaoudi, M.; O'Keeffe, M.; Yaghi, O. M. *Nature* **1999**, *402*, 276.
(39) Li, H.; Eddaoudi, M.; Groy, T. L.; Yaghi, O. M. *J. Am. Chem. Soc.* **1998**, *120*, 571.
(40) Harris, J. G.; Yung, K. H. *J. Phys. Chem.* **1995**, *99*, 12021.
(41) Makrodimitris, K.; Papadopoulos, G. K.; Theodorou, D. N. *J. Phys. Chem. B* **2001**, *105*, 777.
(42) Mayo, S. L.; Olafson, B. D.; Goddard, W. A., III *J. Phys. Chem.* **1990**, *94*, 8897.
(43) Macedonia, M. D.; Maginn, E. J. *Mol. Phys.* **1999**, *96*, 1375.
(44) Goj, A.; Sholl, D. S.; Akten, E. D.; Kohen, D. *J. Phys. Chem. B* **2002**, *106*, 8367.
(45) Frenkel, D.; Smit, B. *Understanding Molecular Simulation: From Algorithms to Applications*; Academic Press: London, 1996.
(46) Heuchel, M.; Snurr, R. Q.; Buss, E. *Langmuir* **1997**, *13*, 6795.
(47) Perry, R. H.; Chilton, C. H. *Chemical Engineer's Handbook*, 5th ed.; McGraw-Hill: New York, 1973.
(48) Doulsin, D. R.; Harrison, R. H.; Moore, R. T. *J. Phys. Chem.* **1967**, *71*, 3477.
(49) *NIST Chemistry Webbook*; National Institute of Standards and Technology: Gaithersburg, MD; http://webbook.nist.gov/chemistry.
(50) Theodorou, D. N.; Snurr, R. Q.; Bell, A. T. Molecular Dynamics and Diffusion in Microporous Materials. In *Comprehensive Supramolecular Chemistry*; Alberti, G., Bein, T., Eds.; Pergamon Press: New York, 1996; Vol. 7, p 507.
(51) Maginn, E. J.; Bell, A. T.; Theodorou, D. N. *J. Phys. Chem.* **1993**, *97*, 4173.
(52) Goodbody, S. J.; Watanabe, K.; MacGowan, D.; Walton, J. P. R. B.; Quirke, N. *J. Chem. Soc., Faraday Trans.* **1991**, *87*, 1951.
(53) Rajappa, C.; Yashonath, S. *J. Chem. Phys.* **1999**, *110*, 5960.
(54) Kar, S.; Chakravarty, C. *J. Phys. Chem. B* **2000**, *104*, 709.
(55) Tunca, C.; Ford, D. M. *J. Chem. Phys.* **1999**, *111*, 2751.
(56) Tunca, C.; Ford, D. M. *J. Phys. Chem. B* **2002**, *106*, 10982.
(57) Tunca, C.; Ford, D. M. *Chem. Eng. Sci.* **2003**, *58*, 3373.

(58) Sokhan, V. P.; Nicholson, D.; Quirke, N. *J. Chem. Phys.* **2004**, *120*, 3855.
(59) Jiang, L.; Biegler, L. T.; Fox, V. G. *AIChE J.* **2003**, *49*, 1140.
(60) Ko, D.; Siriwardane, R.; Biegler, L. T. *Ind. Eng. Chem. Res.* **2003**, *42*, 339.
(61) Skoulidas, A. I.; Bowen, T. C.; Doelling, C. M.; Falconer, J. L.; Noble, R. D.; Sholl, D. S. *J. Membr. Sci.* **2003**, *227*, 123.
(62) Gadre, S. A.; Ritter, J. A. *Ind. Eng. Chem. Res.* **2002**, *41*, 4353.
(63) Bhatia, S. K.; Nicholson, D. *Phys. Rev. Lett.* **2003**, *90*, 016105.
(64) Arya, G.; Chang, H.-C.; Maginn, E. J. *Phys. Rev. Lett.* **2003**, *91*, 026102.
(65) Hinds, B. J.; Chopra, N.; Rantell, T.; Andrews, R.; Gavalas, V.; Bachas, L. G. *Science* **2004**, *303*, 62.
(66) Schoen, M.; Hoheisel, C. *Mol. Phys.* **1984**, *52*, 1029.
(67) Ramprasad, G.; Das, T. R.; Mukherjee, A. K. *J. Chem. Eng. Jpn.* **1991**, *24*, 389.
(68) Taylor, W. L.; Cain, D. *J. Chem. Phys.* **1983**, *78*, 6220.